Progress In Electromagnetics Research C, Vol. 129, 127–141, 2023

Design and Optimization of a Reverse Salient Pole Flux Controlled Permanent Magnet Motor

Xiping Liu, Wenrui Wang*, Siting Zhu, Yun Gao, and Jingya Fu

Abstract—This paper presents a novel reverse salient pole flux controllable permanent magnet (RSP-FCPM) motor topology, and the motor rotor is reasonably designed to have reverse salient pole characteristics and flux controllable characteristics. After selecting the design variables for the RSP-FCPM motor using sensitivity analysis, a multi-objective genetic algorithm is applied to multi-objective optimization. The optimized RSP-FCPM motor is simulated and compared, and the results show that the optimal RSP-FCPM motor has better flux weakening capability, wider speed range, and constant power output area. It can solve the problem of difficult flux changes of the conventional interior permanent magnet motor, and other electromagnetic performances are also more advantageous. To confirm the reliability of the rotor structure during operation, a stress analysis of the rotor is performed, and the results show that the rotor structure can fully withstand high-speed and high-temperature conditions and can operate safely and stably. It also has more advantages in noise performance, which has great prospects for application in the field of electric vehicles.

1. INTRODUCTION

In recent years, because of the concept of carbon neutrality and people's attention to environmental issues, electric vehicles have gradually taken over the position of traditional fuel vehicles with their advantages of low pollution, high efficiency, low cost, and have been widely promoted in the fields of passenger cars and commercial vehicles. At present, the motors applied in electric vehicles are Direct Current motors, Induction motors, Switched Reluctance motors, and Permanent Magnet motors. Among them, Conventional Interior Permanent Magnet (CIPM) motor has been widely used in the field of electric vehicles because of its high operating efficiency, fast dynamic response, small cogging torque, and simple structure.

However, CIPM motor also has very obvious disadvantages. Because of the difficulty of adjusting the flux of its permanent magnets (PMs), the poor flux weakening capability of a CIPM motor makes it difficult to expand the speed. Moreover, under high current and high-temperature operation, the permanent magnet may suffer from a high risk of irreversible demagnetization [1–6], which will limit the development of permanent magnet motors in the field of electric vehicles in the future. To solve the above problems, many scholars have conducted in-depth research and experiments and proposed many novel motor topologies. Some scholars have proposed the concept of Memory motor [7–10], which uses current pulses to change the magnetization level of permanent magnets to regulate the magnetic flux, but there are problems such as large back-electromotive force distortion rate, large torque ripple, and unstable magnetization. In addition, a Flux-Intensifying Permanent Magnet motor [11–14], also called reverse salient pole motor, has been proposed. Its flux weakening capability is increased by increasing the d-axis inductance so that $L_d > L_q$. In [15–18], a Hybrid Excitation motor was proposed, which

Received 29 November 2022, Accepted 11 January 2023, Scheduled 29 January 2023

* Corresponding author: Wenrui Wang (wwr1306543853@gmail.com).

The authors are with the College of Electrical and Automation, Jiangxi University of Science and Technology, Ganzhou 341000, China.

is composed of a permanent magnet and an excitation winding to generate a magnetic field together and can regulate the air-gap magnetic field by excitation winding, but its structure is more complex than CIPM motor, and the design difficulty increases. In [19–21], a variable flux motor concept was proposed to achieve indirect control of the air-gap flux by adding a leakage bridge and controlling the q-axis current.

In this paper, a novel topology of reverse salient pole flux controllable permanent magnet (RSP-FCPM) motor is proposed. It can combine reverse salient pole motor characteristics and flux controllable characteristics, and through a reasonable design, it has a wide flux-controlled range and a low risk of irreversible demagnetization of the permanent magnets. Its electromagnetic performance is improved by multi-objective optimization and compared with a CIPM motor and the motor before optimization. Finally, stress analysis is performed to confirm its reliability at high-speed operation.

2. TOPOLOGY AND PRINCIPLES OF MOTOR

2.1. Topology Design

This paper presents a novel reverse salient pole flux controllable permanent magnet (RSP-FCPM) motor topology, which is evolved based on a CIPM motor. Fig. 1 shows the topology model of the CIPM motor and RSP-FCPM motor. The two motors have the same stator structure and winding distribution, and the main design parameters are shown in Table 1. Fig. 2 shows the evolution of a CIPM motor into an RSP-FCPM motor. To achieve the characteristics of reverse salient pole, two methods are adopted to change the CIPM motor. One is to segment the permanent magnet of the CIPM motor and add two magnetic bridges to each magnetic pole to increase the d-axis inductance; the other is to set a large

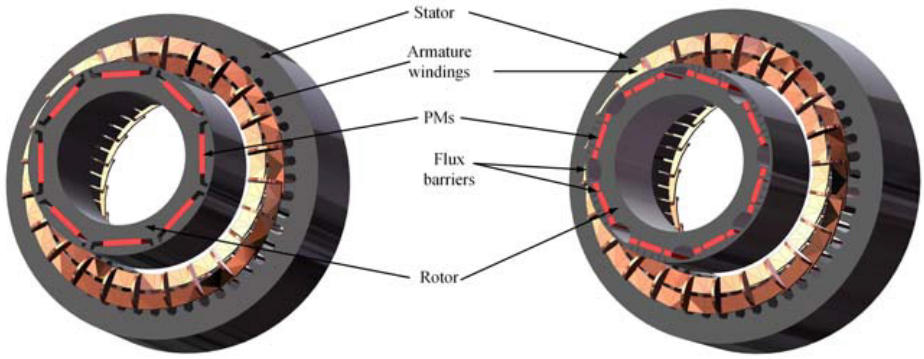

Figure 1. The CIPM motor and RSP-FCPM motor topology model.

Table 1. Key design parameters of the two motors.

Parameters	CIPM	RSP-FCPM
Stator outer/inner diameter (mm)	269.24/161.9	269.24/161.9
Rotor outer/inner diameter (mm)	160.4/110.64	160.4/110.64
Stack length (mm)	83.82	83.82
Rated speed (rpm)	1000	1000
Air-gap length (mm)	0.75	0.75
Numbers of slot/pole/turns	48/8/18	48/8/18
PM cross-sectional area (mm^2)	82	82
PM material	N35AH	N35AH
Widen of magnetic bridge (mm)	2	2

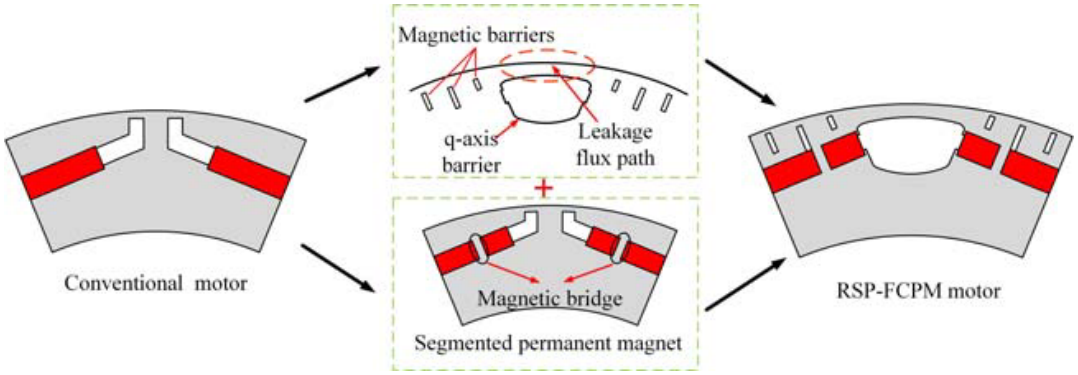

Figure 2. Rotor evolution.

magnetic barrier on the q-axis to reduce the q-axis inductance. At the same time, some suitable bar magnetic barriers are set above the permanent magnet, which can adjust the magnetic circuit and reduce the torque ripple and radial electromagnetic force. To achieve the characteristics of flux controllable, a flux leakage bridge is designed above the magnetic barrier of the q-axis to realize the control of flux. This flux leakage bridge can be controlled by changing the q-axis current to control its saturation level, so that the air-gap flux can be controlled. When the motor needs to run at high speed, the leakage flux can be increased by reducing the q-axis current, which reduces the reverse current required for magnetic weakening, thus reducing the risk of irreversible demagnetization of the permanent magnets.

2.2. Operation Principles

To better analyze the design principle of the RSP-FCPM motor, the magnetic circuit can be concretized as Fig. 3 for theoretical analysis. From the figure, the inductance of the RSP-FCPM motor can be expressed as:

$$L_d = \frac{N^2}{R_s + R_g + \dfrac{R_c\left(R_{pm} + R_r\right)}{R_{pm} + R_r + R_c}} \tag{1}$$

$$L_q = \frac{N^2}{R_s + R_g + R_r + R_b + R_c} \tag{2}$$

where R_s, R_g, R_r, R_b, and R_{pm} respectively represent the reluctance of stator, air gap, rotor, q-axis magnetic barrier, and the permanent magnet, and N is the number of turns of winding. In order to achieve $L_d > L_q$, the motor is designed mainly to reduce L_q by increasing R_b in the large magnetic barrier of the q-axis and to increase the inductance of the d-axis by segmenting permanent magnets.

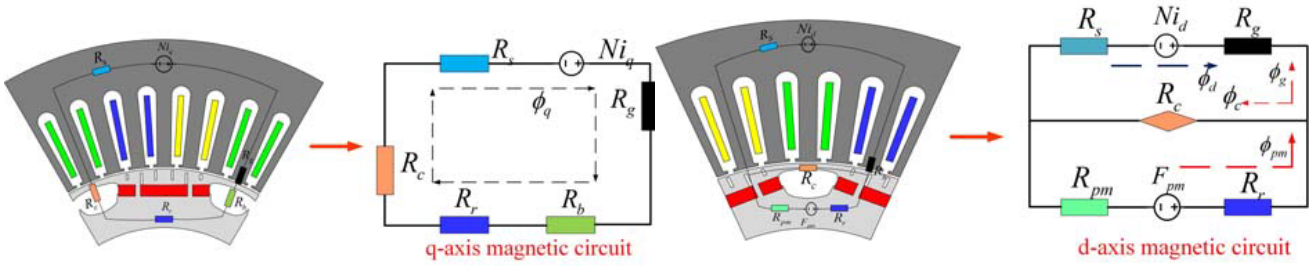

Figure 3. Magnetic circuit model of q-axis and d-axis.

Based on the d-axis magnetic circuit, its flux controllable characteristics can be expressed as:

$$R_c = \frac{Ni_q}{\phi_q} - R_s - R_g - R_b - R_r \tag{3}$$

$$\phi_c = \phi_{pm} - \phi_g = \frac{(R_g + R_s) F_{pm} - R_s N i_d}{R_c (R_r + R_{pm}) + (R_c + R_r + R_{pm}) (R_s + R_g)} \tag{4}$$

where F_{pm} is the magnetomotive force of the permanent magnet; i_d and i_q are the d-axis and q-axis currents; Ni_d and Ni_q represent the magnetomotive forces of d-axis and q-axis; φ_{pm}, φ_c, and φ_g represent permanent magnet flux, magnetic leakage bridge flux, and the air-gap flux. It can be seen from formula (3) that the flux leakage bridge reluctance R_c can be changed by controlling the q-axis current. From formula (4), it can be seen that when R_c is changed, the value of the flux leakage φ_c can be changed, indicating that the magnetic flux can be controlled by controlling the q-axis current. In this article, this method is used to achieve flux control.

3. PERFORMANCE OPTIMIZATION OF RSP-FCPM MOTOR

Due to the multiple and complex working conditions of the electric vehicle, the requirements of the motor under different working conditions are different, so the multi-objective optimization of this motor is required. The optimization objectives are selected reasonably according to the requirements of the actual situation and the deficiencies of the initial motor, and the corresponding constraints are set. Because of the large number of design variables of the motor structure, to reduce the workload of optimization, this paper uses the sensitivity analysis method to stratify the design variables; the parameters with low integrated sensitivity are output by initial values; and those with high sensitivity coefficients are then optimized using the genetic factor algorithm to obtain the optimal points. Finally, the model is built according to the obtained optimal point and compared with the initial RSP-FCPM motor and the CIPM motor in terms of performance. The specific optimization process is shown in Fig. 4.

3.1. Selection of the Optimized Objectives and Design Variables

The traction motor must be able to output enough torque to meet the heavy load climbing conditions of the electric vehicle. More magnetic barriers can affect the stable operation of the motor, so it is necessary to reduce the torque ripple of the engine by optimizing the rationalization of the magnetic circuit [22]. In order for the motor to operate in the flux enhancement region, this requires the RSP-FCPM motor with a large inverse convex pole ratio and also a large d-axis flux variation range to improve the control range over the flux. Therefore, the output average torque T_{avg}, torque ripple T_{rip}, reverse salient ratio λ, and d-axis flux variation range Ψ are selected as optimization objectives.

The output average torque T_{avg} and torque ripple K_{rip} of the RSP-FCPM motor can be expressed as:

$$T_{avg} = \frac{3}{2} p \left[\varphi_{pm} i_q + (L_d - L_q) i_d i_q\right] \tag{5}$$

$$T_{rip} = \frac{T_{\max} - T_{\min}}{T_{avg}} \times 100\% \tag{6}$$

where φ_{pm} is the PM flux linkage; p is the pole pair number; L_d and L_q are d-axis inductance and q-axis inductance.

$T_{\max}$ and $T_{\min}$ are the maximum and minimum torques.

In addition, the reverse salient ratio λ and d-axis flux variation range Ψ can be expressed as:

$$\lambda = \frac{L_d}{L_q} \tag{7}$$

$$\psi = \frac{\varphi_{\max} - \varphi_{\min}}{\varphi_{\min}} \times 100\% \tag{8}$$

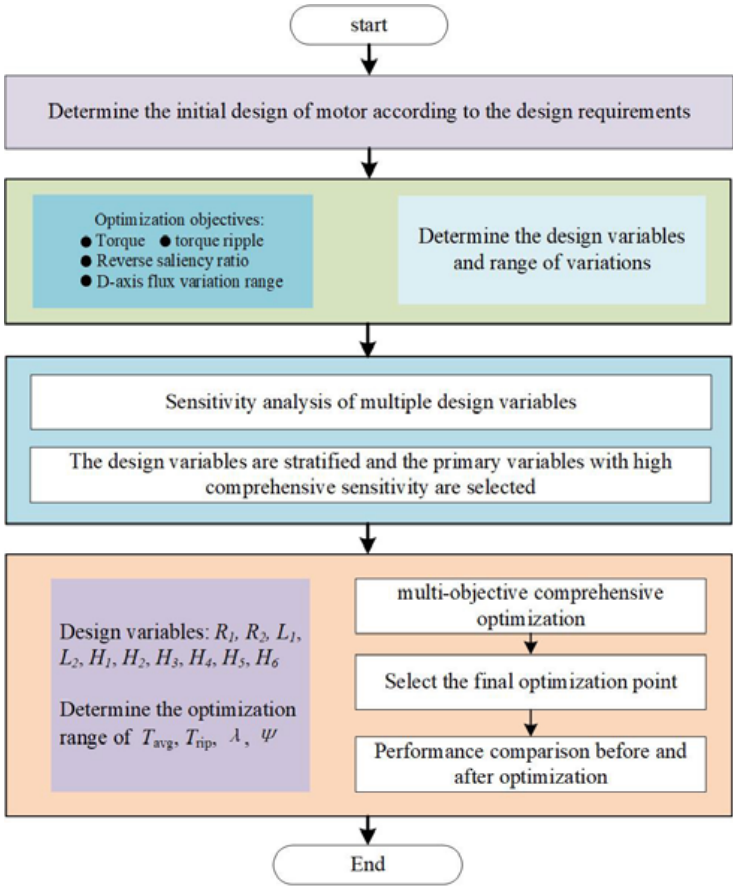

Figure 4. Optimization flowchart of the RSP-FCPM motor.

where $\varphi_{\max}$ and $\varphi_{\min}$ represent the maximum and minimum flux linkage flowing through the d-axis, respectively.

Through the preliminary consideration of the influence of the optimization target, a part of the rotor structure parameters were selected as the design parameters, as shown in Fig. 5, and the range of variation of the design variables is shown in Table 2.

Table 2. Variation ranges of the design variables.

Design variables	Variation ranges
Distance from the PM to the center of the rotor circle $\boldsymbol{R_1}$	[67 mm, 69 mm]
Distance from the q-axis magnetic barrier to the center of the rotor circle $\boldsymbol{R_2}$	[68 mm, 70 mm]
Horizontal position of 1st magnetic barrier $\boldsymbol{L_1}$	[3 mm, 5.5 mm]
Horizontal position of the 3rd magnetic barrier $\boldsymbol{L_2}$	[3 mm, 6 mm]
The length of 1st magnetic barrier $\boldsymbol{H_1}$	[2 mm, 4.5 mm]
Distance from 1st magnetic barrier to the PM $\boldsymbol{H_2}$	[1 mm, 2.5 mm]
The length of 2nd magnetic barrier $\boldsymbol{H_3}$	[3.5 mm, 5 mm]
Distance from 3rd magnetic barrier to the PM $\boldsymbol{H_4}$	[1 mm, 2.5 mm]
Distance from q-axis magnetic barrier to rotor outer diameter $\boldsymbol{H_5}$	[1.5 mm, 3 mm]
Height of q-axis magnetic barrier $\boldsymbol{H_6}$	[5 mm, 7 mm]

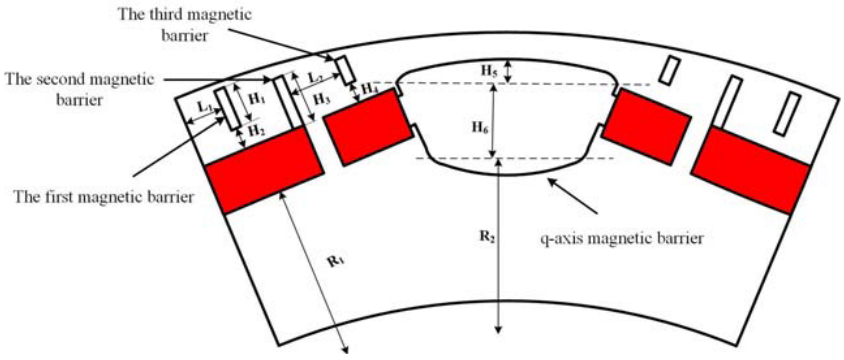

Figure 5. Design variables of the RSP-FCPM motor rotor structure.

3.2. Sensitivity Analysis

The sensitivity of each design variable to different optimization objectives is also different. Since the number of design variables is large, and the sensitivity to different optimization objectives is different, a comprehensive sensitivity calculation method is given to reasonably filter out the design variables that have a greater impact on each optimization objective

$$S_{cpn}(x_i) = K_{avg}|S_{avg}(x_i)| + K_{rip}|S_{rip}(x_i)| + K_{\lambda}|S_{\lambda}(x_i)| + K_{\psi}|S_{\psi}(x_i)| \tag{9}$$

$$K_{avg} + K_{rip} + K_{\lambda} + K_{\psi} = 1 \tag{10}$$

where S_{cpn} is the comprehensive sensitivity; K_{avg}, K_{rip}, K_{λ}; K_{φ} are the weights of different optimization objectives, and they must satisfy the relation formula (10). $|S_{avg}(x_i)|$, $|S_{rip}(x_i)|$, $|S_{\lambda}(x_i)|$, and $|S_{\Psi}(x_i)|$ are absolute values of sensitivity of design variables to different optimization objectives. In order to ensure the normal start-up and stable operation of the electric car wash, the weight coefficients of output torque T_{avg} and torque ripple T_{rip} are both set to 0.3, which also means that these two optimization objectives are equally important in the whole system. Both the reverse saliency ratio λ and d-axis flux variation range Ψ can widen the speed range of the motor at high speed, and these two optimization objectives are considered to be of the same importance. The weight coefficients of both are set to 0.2 in order to make the sum of the weight coefficients equal to 1. The specific arithmetic results are shown in Table 3.

Table 3. Sensitivity and integrated correlation coefficient.

Design variables	Optimization goals				S_{cpn}
	T_{avg}	T_{rip}	λ	Ψ	
	$K_{avg} = 0.3$	$K_{rip} = 0.3$	$K_{\lambda} = 0.2$	$K_{\Psi} = 0.2$	
R_1	3.76	−7.91	16.57	−5.59	7.933
R_2	19.96	8.87	−12.97	−15.83	14.409
L_1	0.33	−18.50	−0.50	0.33	5.815
L_2	1.15	−19.90	0.33	−0.41	6.463
H_1	3.22	−12.09	9.78	3.06	7.161
H_2	−0.06	−4.01	0.16	0.21	1.295
H_3	2.27	27.39	5.20	−5.19	10.976
H_4	−0.34	−4.83	0.88	−0.38	1.803
H_5	21.87	−8.48	−17.39	−15.00	15.583
H_6	25.59	13.00	−17.22	−20.12	19.045

According to the calculation results of comprehensive sensitivity, the design variables can be divided into the following two levels

Lever 1: Nonsensitive: $S_{cpn} < 7$; L_1, L_2, H_2, H_4

Lever 2: Stongly sensitive: $S_{cpn} \geq 7$; R_1, R_2, H_1, H_3, H_5, H_6

The original values of the design variables in Level 1 are retained, and the design variables in Level 2 are selected for optimization.

3.3. Objective Optimization

The response surface optimization (RSM) algorithm is used to find a series of design points that satisfy the target boundary conditions as candidate points. Based on this, a multi-objective optimization model is proposed to select the best point from many candidate points [23]. The model is given as follows:

$$\begin{cases} g(x_i)_{\min} = K_{avg}\frac{T^*_{avg}(x_i)}{T'_{avg}(x_i)} + K_{rip}\frac{T'_{rip}(xi)}{T^*_{rip}(xi)} + K_\lambda\frac{\lambda^*(x_i)}{\lambda'(x_i)} + K_\varphi\frac{\varphi^*(x_i)}{\varphi'(x_i)} \\ \text{Constraints}: \ T_{avg} \geq 70\,\text{Nm};\ T_{rip} \leq 10\%;\ \lambda \geq 1.2;\ \varphi \geq 30\% \end{cases} \tag{11}$$

where $T'_{avg}(x_i)$, $T'_{rip}(x_i)$, $\lambda'(x_i)$, and $\Psi'(x_i)$ are the average output torque, torque ripple, reverse salient ratio, and d-axis flux variation range corresponding to the candidate points, respectively. $T^*_{avg}(x_i)$, $T^*_{rip}(x_i)$, $\lambda^*(x_i)$, and $\Psi^*(x_i)$ are their boundary values, respectively. The constraints made on the boundary values of each optimization objective according to the demand for the motor are shown in Equation (11). When function $g(x_i)_{\min}$ is minimized, the corresponding trade-off design point is the globally optimal point. Fig. 6 shows a series of optimization points obtained according to the functions and constraints, then the global optimal point is obtained by multi-objective genetic algorithm. The red point is the global optimal solutions, and the specific optimization results are shown in Table 4.

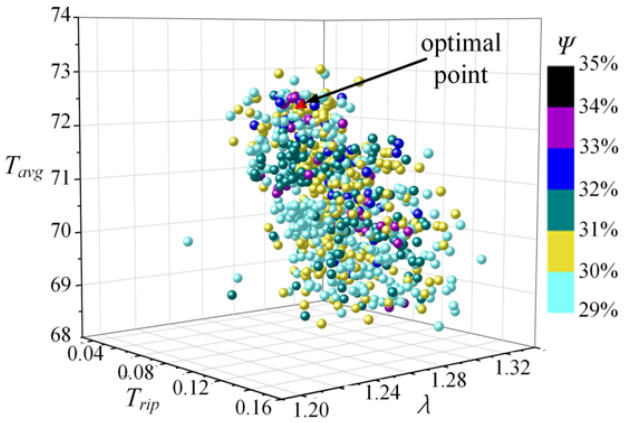

Figure 6. Optimization results.

4. PERFORMANCES ANALYSIS AND COMPARISON

To verify the design concept of the RSP-FCPM motor and the effect of the optimization, the electromagnetic performances of the RSP-FCPM motor before and after optimization will be compared in detail. Since the motor is an improvement of the CIPM motor, the CIPM motor is also added as a comparison so that the performance of the RSP-FCPM motor can be better evaluated.

Table 4. Optimization results of design variables.

RSP-FCPM		Initial values	Optimal values
Design variables	R_1	67.80 mm	68.50 mm
	R_2	68.50 mm	69.40 mm
	H_1	3.50 mm	4.10 mm
	H_3	4.50 mm	5.00 mm
	H_5	2.50 mm	2.25 mm
	H_6	5.00 mm	6.00 mm
Optimization results	T_{avg}	67.3 Nm	73.6 Nm
	T_{rip}	18.16%	6%
	λ	1.24	1.30
	Ψ	27.12%	33.75%

4.1. Flux Characteristic

Flux controllable characteristic is one of the important characteristics of the RSP-FCPM motor, then it is very necessary to analyze the magnetic flux characteristics of the RSP-FCPM motor. Fig. 7(a) and Fig. 7(b) show the magnetic field distribution of the RSP-FCPM motor under no-load and heavy-load conditions, respectively. From Fig. 7, it can be seen that when RSP-FCPM motor is running at no-load, there are relatively more magnetic lines passing through the adjacent permanent magnets and leakage flux to form a leakage circuit due to the existence of leakage bypass, and the remaining magnetic lines are flowing through the air gap to the stator. From Fig. 8, it can be seen that when the RSP-FCPM motor is under heavy load by adding a larger q-axis current, most of the magnetic lines flow to the stator instead of to the adjacent poles as in the no-load condition. This is because the action of the q-axis current makes the leakage bridge magnetically saturated, thus reducing the leakage flux, which allows the generated torque to meet the actual demand.

Figure 7(c) shows the d-axis flux variation range. From the figure, it can be seen that as the q-axis current increases, the d-axis flux flowing to the stator also increases, and it has a flux controllable range of 33%. Since both the initial RSP-FCPM motor and the optimal RSP-FCPM motor have leakage bridges, the d-axis flux can be controlled by the q-axis current, but the control range of the optimized RSP-FCPM motor is increased by 22% compared to the initial RSP-FCPM motor, which proves that this optimization method has excellent results.

4.2. Inductance Characteristics

The reverse salient pole characteristic is another important characteristic of the RSP-FCPM motor, which is more related to the inductance, so it is also necessary to analyze the inductance of the RSP-FCPM motor. Fig. 8(a) shows the difference in inductance characteristics between the CIPM motor and RSP-FCPM motor. The d-axis inductance of the RSP-FCPM motor is larger than the q-axis inductance, which is the opposite of the inductance characteristics of the CIPM motor, and the d-axis inductance of the RSP-FCPM motor is also larger than the d-axis inductance of the CIPM motor. When the motor is accelerated by weak magnetism, the current required in the opposite direction is related to the d-axis inductance. Since the d-axis inductance of the RSP-FCPM motor is larger, the current required in the opposite direction for weak magnetic control is smaller, which results in a lower risk of irreversible demagnetization of the permanent magnets and higher reliability of the motor. Their inductance characteristics also verify the feasibility of increasing the d-axis inductance and reducing the q-axis inductance by adding magnetic barriers.

Figure 8(b) shows the variation of the reverse saliency ratio with different q-axis currents for the CIPM motor, the initial RSP-FCPM motor, and the optimal RSP-FCPM motor. It can be seen from the figure that the optimal RSP-FCPM motor's reverse salient ratio is always greater than the CIPM motor and the initial RSP-FCPM motor at different currents, which indicates that the optimal RSP-

FCPM motor works better in the magnetic field enhancement state and has better reverse salient pole characteristics. The effectiveness of the optimization method is also verified.

4.3. Torque Performance

Figure 9(a) shows the output torque at different current angles. As can be seen from the figure, the current angle for the conventional motor to produce the maximum output torque is 29°; the current angle of the maximum output torque of the initial RSP-FCPM motor is −1°; and after optimization of the reverse salient ratio, the maximum output torque current angle of the optimal RSP-FCPM motor is −4°. This is because the RSP-FCPM motor has the characteristic of $L_d > L_q$, so it can output positive reluctance torque, which makes the maximum output torque of the RSP-FCPM motor generated in the

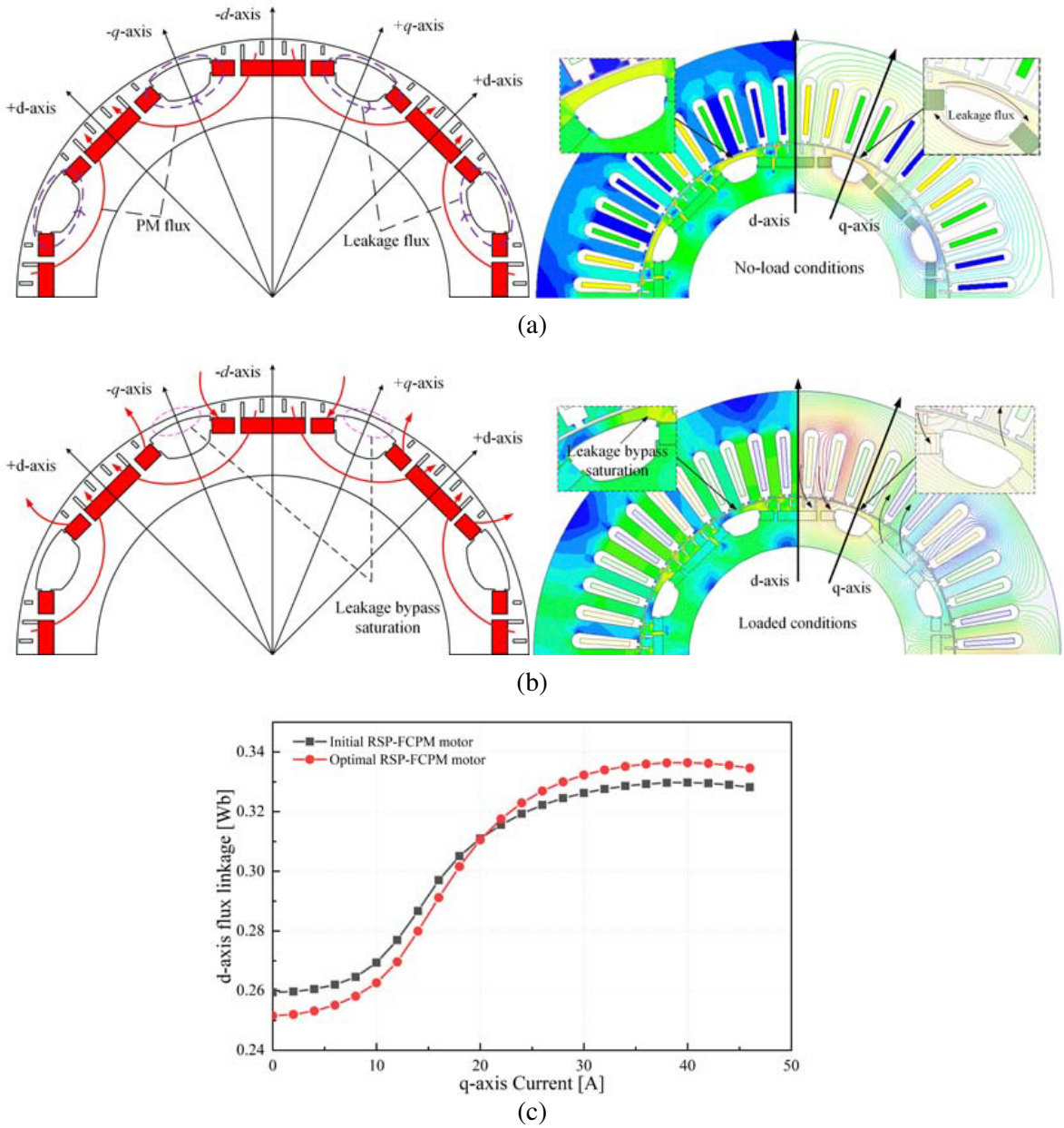

Figure 7. Flux characteristics of the RSP-FCPM motor. (a) No-load condition. (b) Heavy-load condition. (c) Controllable range of *d*-axis flux.

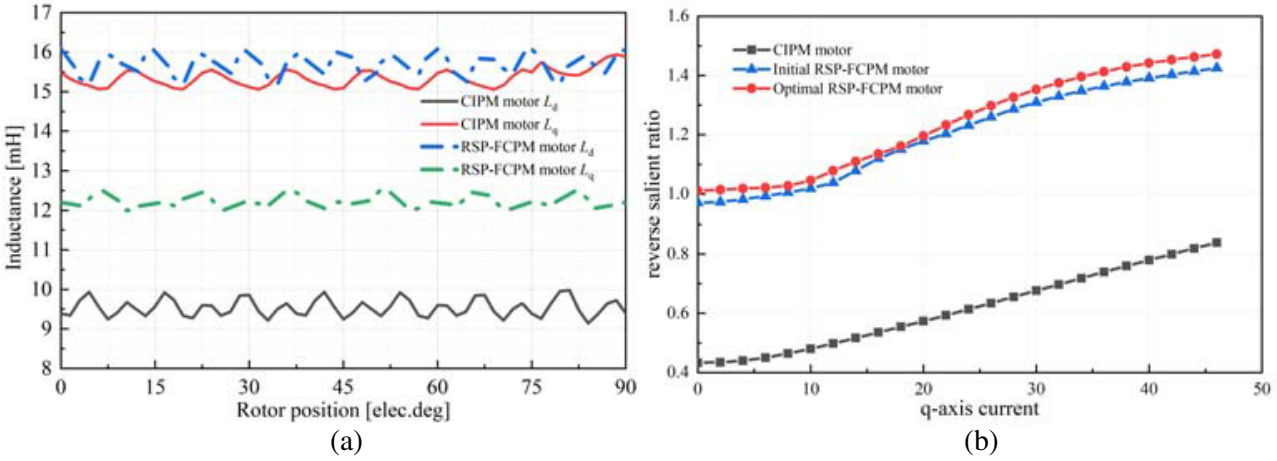

Figure 8. Inductance characteristic. (a) CIPM motor and RSP-FCPM motor inductance. (b) Reverse saliency ratio.

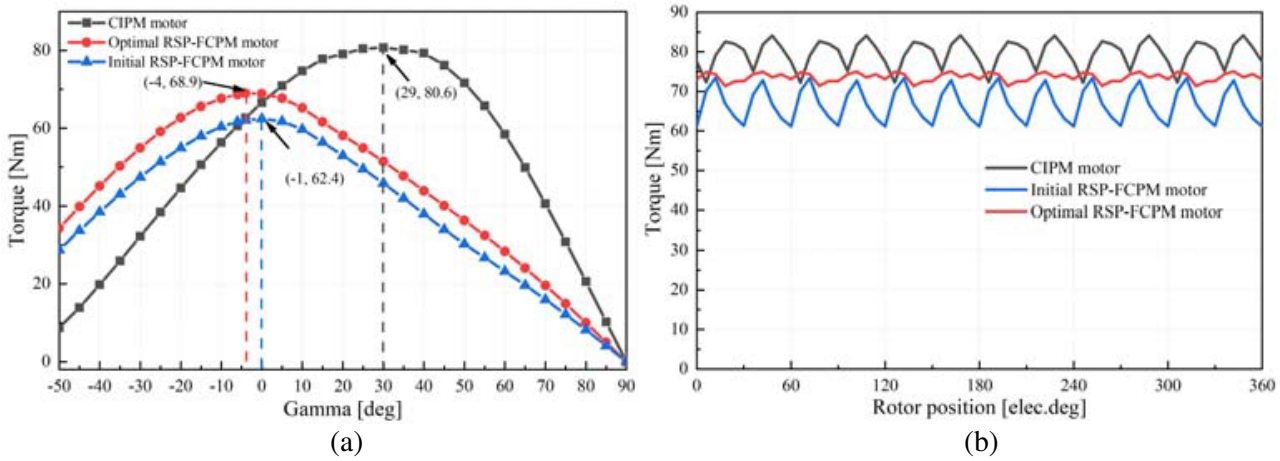

Figure 9. Torque characteristic of the three motors. (a) Output torque at different current angles. (b) Output torque and output ripple.

flux increase interval. In contrast, since the CIPM motor has the characteristic of $L_d < L_q$, its maximum output torque is generated in the weak magnetization interval, which means that the operating point of the permanent magnets in the CIPM motor under load conditions is lower than that of the RSP-FCPM motor, and the risk of irreversible demagnetization is higher.

Figure 9(b) shows the output torque of the CIPM motor, initial RSP-FCPM motor, and optimal RSP-FCPM motor. It can be seen that after multi-objective optimization, the torque ripple of the RSP-FCPM motor is reduced from 18% to 6%, and the output torque is increased by 7%. However, it can also be seen that because of the leakage bypass, some of the flux leaks, making the output torque of the RSP-FCPM motor lower than the CIPM motor.

4.4. Speed and Constant Output Power Range

The design concept of the motor is mainly to make it have better flux weakening capability to achieve a wider speed range, so it is necessary to analyze and compare the flux weakening capability and speed range of the RSP-FCPM motor. Fig. 10(a) shows the torque-speed envelopes of the CIPM motor, the initial RSP-FCPM motor, and the optimal RSP-FCPM motor. It is manifested from the figure that although the torque of the RSP-FCPM motor is smaller than the CIPM motor, its weak

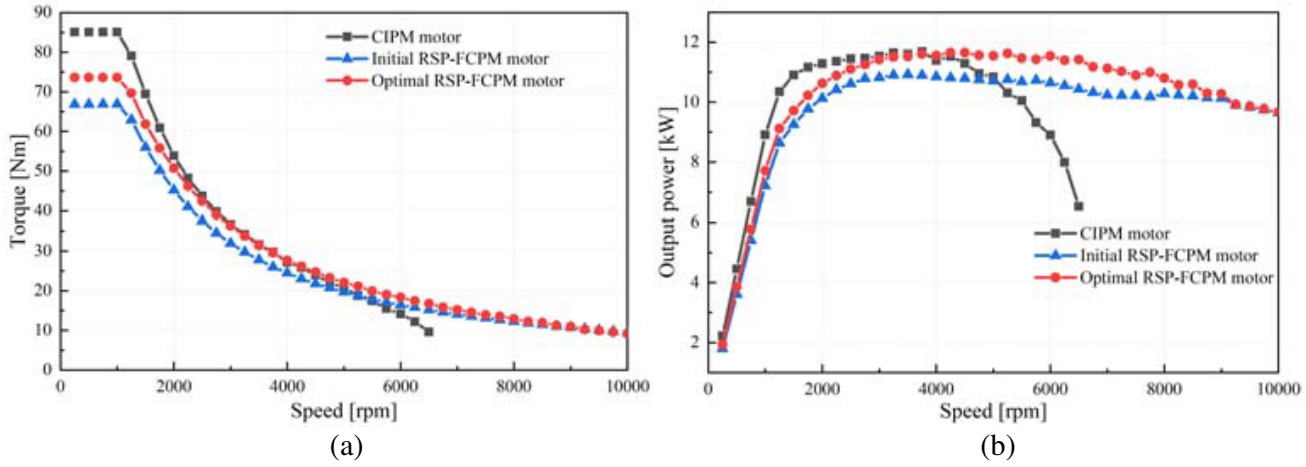

Figure 10. Torque-speed and output power-speed characteristics of the three motors. (a) Torque-speed envelops. (b) Output power-speed envelops.

magnetic capability is better than the CIPM motor because of the leakage bypass, so the speed expansion capability is also better. The initial RSP-FCPM motor also has a better speed expansion capability than the CIPM motor because it has a similar structure, but the output torque of the optimal RSP-FCPM motor is higher.

Figure 10(b) shows the output power performance of the three motors. As can be seen, the maximum output powers of both the CIPM motor and optimal RSP-FCPM motor are close to 12 kW, but the constant power output region of the optimal RSP-FCPM motor is wider than that of the CIPM motor. Based on the above analysis, it can be seen that the RSP-FCPM motor with reverse salient pole characteristics and flux-controlled characteristics has better high-speed operation performance and speed regulation range.

4.5. Loss and Efficiency

As the largest energy-consuming component of an electric vehicle, the efficiency of the motor directly affects the range of the vehicle, and the higher the loss of the motor is, the lower its efficiency will be. Fig. 11 gives the core loss map of the CIPM motor and RSP-FCPM motor at the base speed of 1000 rpm. It is manifested from the figure that no matter the RSP-FCPM motor before or after optimization, the core loss at the base speed is not much different, but in the high-speed region, the RSP-FCPM motor has many magnetic barriers on the rotor and has a lot of leakages, so the core loss will be smaller than

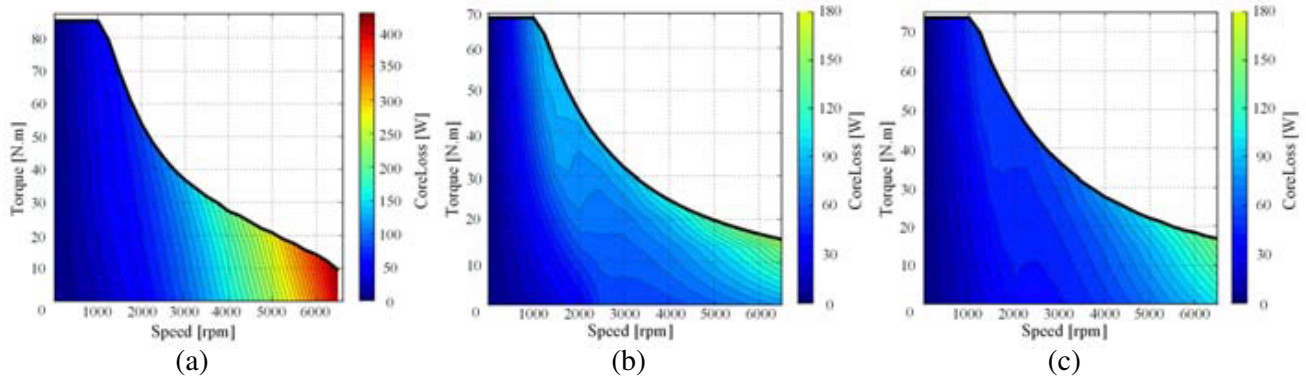

Figure 11. Core losses of the three motors. (a) CIPM motor. (b) Initial RSP-FCPM motor. (c) Optimal RSP-FCPM motor.

that of the CIPM motor. The core loss is 400 w when the CIPM motor reaches the limit speed, but the core loss of the RSP-FCPM motor is only 180 w. The temperature change of the motor has a great relationship with the core loss, so it can be concluded that the temperature rise of the RSP-FCPM motor at high speed is lower than that of the CIPM motor.

Figure 12 shows the efficiency maps of the three motors. From the figure it can be seen that their maximum efficiency is relatively high, but the optimized motor efficiency of 98% of the region can reach 2800 rpm, while the CIPM motor and the optimization of the former motor can only be in the range of 2250 rpm and 2400 rpm, respectively, and the efficiency of 91% of the region above the optimal RSP-FCPM motor is also higher. This is because the optimal RSP-FCPM motor has better weak magnetic capability and flux controllable characteristics, which can reduce losses, thus allowing the motor to achieve a wide range of speed expansion and a wide range of high-efficiency areas.

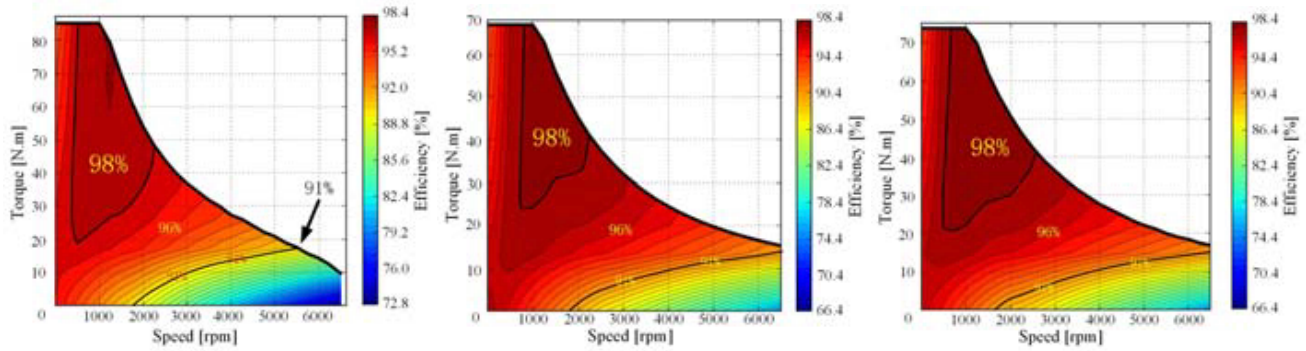

Figure 12. Efficiencies of the three motors. (a) CIPM motor. (b) Initial RSP-FCPM motor. (c) Optimal RSP-FCPM motor.

4.6. Stress Analysis

To achieve the flux controlled characteristics and reverse salient pole characteristics, the RSP-FCPM motor rotor has several magnetic barriers and bridges. This makes the magnetic barriers and bridges weaker than the rest of the rotor, and they are susceptible to deformation and fracture during high-speed operation. Therefore, the mechanical strength of the motor rotor needs to be simulated and analyzed to evaluate the safety and reliability of the motor at high speed. Fig. 13 shows the maximum stress and deformation cloud of the rotor at a speed of 10,000 rpm. Since permanent magnets generally operate below 80°C, the simulation temperature is set to 80°C. The maximum stress on the rotor is 228 MPa, which is less than the ultimate stress value of 430 MPa for the core material, and there is no risk of fracture. The maximum deformation value of the rotor is 0.0456 mm, which is less than one-tenth of the air-gap length. Combined with the above analysis, the rotor structure of the optimal RSP-FCPM motor can operate safely and reliably at high speed.

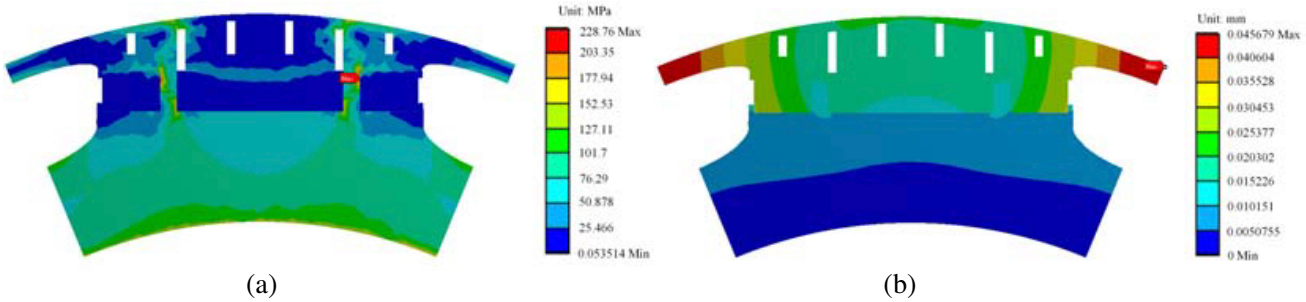

Figure 13. Stress analysis of the optimal RSP-FCPM motor. (a) Stress. (b) Deformation.

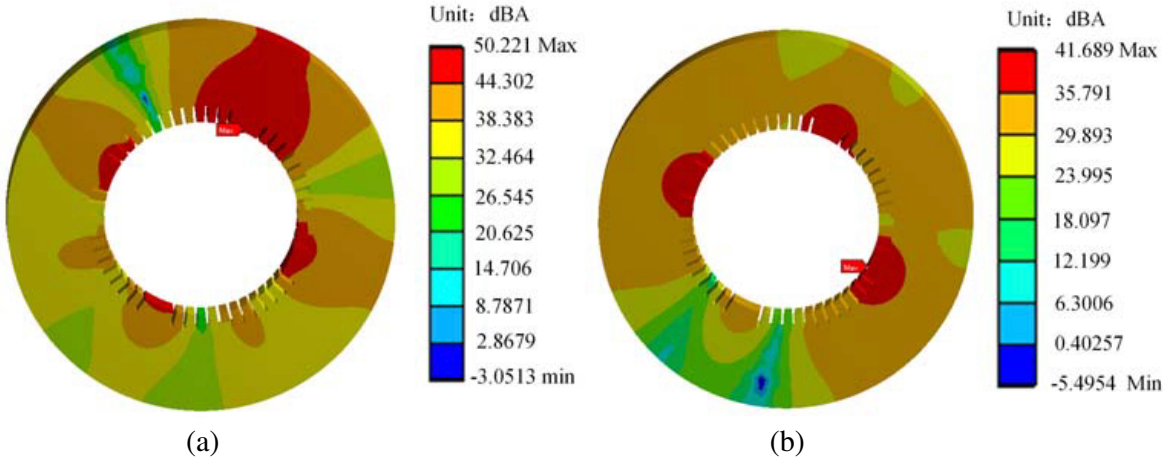

Figure 14. Noise analysis. (a) The CIPM motor. (b) The optimal RSP-FCPM motor.

4.7. Noise Analysis

When designing the RSP-FCPM motor, the magnetic circuit is adjusted by adding some bar magnetic barriers above the permanent magnets, which not only reduces the torque ripple, but also reduces the radial electromagnetic force harmonics of the RSP-FCPM motor, thus reducing the noise of the motor. To verify this possibility, a joint simulation analysis of the CIPM motor and the optimal RSP-FCPM motor was performed using simulation software Maxwell and Workbench to simulate the noise distribution of the two motors in a cylindrical air medium with a radius of 200 mm due to torque ripple and radial electromagnetic forces, and the results are shown in Fig. 14. The noise analysis was performed for both motors with a speed of 10,00 rpm in the same motor housing and air medium. It can be seen from the figure that the maximum noise is generated where the housing and air are in contact, and the further away from the housing, the less noise is generated. The maximum noise of the optimal RSP-FCPM motor is 8 dB lower than the maximum noise of the CIPM motor, which represents that the optimal RSP-FCPM motor has better noise reduction capability and is more advantageous for electric vehicles applications.

5. CONCLUSION

In this paper, a novel topology of RSP-FCPM motor is proposed, in which the reverse salient pole characteristic is achieved by segmenting the permanent magnet with two bridges to increase the d-axis inductance, and then a leakage bypass is set between two adjacent poles to achieve the flux-controllable characteristic. Then the design variables of the RSP-FCPM motor are selected by layers, and finally, a multi-objective optimization is performed to enhance the output torque, reduce the torque ripple, and improve the reverse salient pole ratio and flux controllable range. The electromagnetic performance analysis of the optimal RSP-FCPM motor shows that the optimal RSP-FCPM motor has better flux weakening capability, wider speed range, and constant power output region than the CIPM motor and the initial RSP-FCPM motor. Although the output torque is reduced due to leakage bypass, it has lower losses, a higher efficiency range, a lower risk of irreversible demagnetization, and higher reliability.

To verify the reliability of the rotor structure during operation, a stress analysis of the rotor was performed, and the results show that the rotor can fully withstand high-speed and high-temperature conditions and can operate safely and stably. Finally, the noise analysis and comparison between the optimal RSP-FCPM motor and CIPM motor show that the RSP-FCPM motor has more advantages in terms of noise performance. In summary, the motor proposed in this paper can solve the problem of difficult flux changes in CIPM motors, and after performance analysis and comparison, it proves to have great application prospects in the field of electric vehicles.

ACKNOWLEDGMENT

This work was supported in part by the National Natural Science Foundation of China under Grant 52067008.

REFERENCES

1. Athavale, A., K. Sasaki, B. S. Gagas, T. Kato, and R. D. Lorenz, "Variable Flux Permanent Magnet Synchronous Machine (VF-PMSM) design methodologies to meet electric vehicle traction requirements with reduced losses," *IEEE Transactions on Industry Applications*, Vol. 53, No. 5, 4318–4326, 2017.
2. Babetto, C., G. Bacco, and N. Bianchi, "Synchronous reluctance machine optimization for high-speed applications," *IEEE Transactions on Energy Conversion*, Vol. 33, No. 3, 1266–1273, 2018.
3. Gagas, B. S., K. Sasaki, A. Athavale, T. Kato, and R. D. Lorenz, "Magnet temperature effects on the useful properties of variable flux PM synchronous machines and a mitigating method for magnetization changes," *IEEE Transactions on Industry Applications*, Vol. 53, No. 3, 2189–2199, 2017.
4. Kim, J., J. Choi, K. Lee, and S. Lee, "Design and analysis of surface-mounted-type variable flux permanent magnet motor for wide-speed range applications," *IEEE Transactions on Magnetics*, Vol. 51, No. 1, 1–4, 2015.
5. Zhao, X. and S. Niu, "Design and optimization of a novel slot-PM-assisted variable flux reluctance generator for hybrid electric vehicles," *IEEE Transactions on Energy Conversion*, Vol. 33, No. 4, 2102–2111, 2018.
6. Zhang, S., P. Zheng, T. M. Jahns, L. Cheng, M. Wang, and Y. Sui, "A novel variable-flux permanent-magnet synchronous machine with quasi-series magnet configuration and passive flux barrier," *IEEE Transactions on Magnetics*, Vol. 54, No. 1, 1–5, 2018.
7. Yu, C. and K. T. Chau, "Design, analysis, and control of DC-excited memory motors," *IEEE Transactions on Energy Conversion*, Vol. 26, No. 2, 479–489, 2011.
8. Gong, Y., K. T. Chau, J. Z. Jiang, C. Yu, and W. Li, "Analysis of doubly salient memory motors using preisach theory," *IEEE Transactions on Magnetics*, Vol. 45, No. 10, 4676–4679, 2009.
9. Liu, H., H. Lin, Z. Q. Zhu, M. Huang, and P. Jin, "Permanent magnet remagnetizing physics of a variable flux memory motor," *IEEE Transactions on Magnetics*, Vol. 46, No. 6, 1679–1682, 2010.
10. Chen, D., X. Zhu, L. Quan, Q. Ding, Z. Wang, and M. Cheng, "Electromagnetic performance analysis and fault-tolerant control of new doubly salient flux memory motor drive," *2010 International Conference on Electrical Machines and Systems*, 834–838, 2010.
11. Aoyama, M. and T. Noguchi, "Study and experimental performance evaluation of flux intensifying PM motor with variable leakage magnetic flux," *Electrical Engineering in Japan*, Vol. 207, No. 4, 36–54, 2019.
12. Aljehaimi, A. M. and P. Pillay, "Operating envelopes of the variable-flux machine with positive reluctance torque," *IEEE Transactions on Transportation Electrification*, Vol. 4, No. 3, 707–719, 2018.
13. Chen, Y., X. Zhu, L. Quan, Z. Xiang, Y. Du, and X. Bu, "A V-shaped PM vernier motor with enhanced flux-modulated effect and low torque ripple," *IEEE Transactions on Magnetics*, Vol. 54, No. 1, 1–4, 2018.
14. Limsuwan, N., T. Kato, K. Akatsu, and R. D. Lorenz, "Design and evaluation of a variable-flux flux-intensifying interior permanent-magnet machine," *IEEE Transactions on Industry Applications*, Vol. 50, No. 2, 1015–1024, 2014.
15. Li, J. and K. Wang, "A parallel hybrid excited machine using consequent pole rotor and AC field winding," *IEEE Transactions on Magnetics*, Vol. 55, No. 6, 1–5, 2019.
16. Li, N., X. H. Fu, J. Zhu, M. Y. Lin, G. D. Yang, Y. Kong, et al., "Hybrid-excited series permanent magnet axial field flux switching memory machine," *IEEE Transactions on Applied Superconductivity*, Vol. 29, No. 2, 1–5, 2019.

17. Zheng, Y., L. Wu, Y. Fang, X. Huang, and Q. Lu, "A hybrid interior permanent magnet variable flux memory machine using two-part rotor," *IEEE Transactions on Magnetics*, Vol. 55, No. 7, 1–8, 2019.
18. Yu, J., C. Liu, Z. Song, and H. Zhao, "Permeance and inductance modeling of a double-stator hybrid-excited flux-switching permanent-magnet machine," *IEEE Transactions on Transportation Electrification*, Vol. 6, No. 3, 1134–1145, 2020.
19. Kato, T., M. Minowa, H. Hijikata, K. Akatsu, and R. D. Lorenz, "Design methodology for variable leakage flux IPM for automobile traction drives," *IEEE Transactions on Industry Applications*, Vol. 51, No. 5, 3811–3821, 2015.
20. Aoyama, M. and T. Noguchi, "Study and experimental performance evaluation of flux intensifying PM motor with variable leakage magnetic flux," *Electrical Engineering in Japan*, Vol. 207, No. 4, 36–54, 2019.
21. Fan, W., X. Zhu, L. Quan, W. Wu, L. Xu, and Y. Liu, "Flux-weakening capability enhancement design and optimization of a controllable leakage flux multilayer barrier PM motor," *IEEE Transactions on Industrial Electronics*, Vol. 68, No. 9, 7814–7825, 2021.
22. Huang, L. R., J. H. Feng, S. Y. Guo, Y. F. Li, J. X. Shi, and Z. Q. Zhu, "Rotor shaping method for torque ripple mitigation in variable flux reluctance machines," *IEEE Transactions on Energy Conversion*, Vol. 33, No. 3, 1579–1589, 2018.
23. Zhu, X., J. Huang, L. Quan, Z. Xiang, and B. Shi, "Comprehensive sensitivity analysis and multi-objective optimization research of permanent magnet flux-intensifying motors," *IEEE Transactions on Industrial Electronics*, Vol. 66, No. 4, 2613–2627, 2019.